

Adaptive Energy-Efficient Transmission Power Control For Wearables And Man-Machine Interfaces That Support 5g

Evelyn Rosero^{a*}, Freddy Patricio Ajila Zaquinaula^b, Miguel Escobar^c, Marcelo Calispa^c

^aEscuela Superior Politécnica de Chimborazo, Sede Morona Santiago, Macas, 140101, Ecuador

^bEscuela Superior Politécnica de Chimborazo, Sede Orellana, El Coca, 220001, Ecuador

^cFacultad de Ingeniería Mecánica, Escuela Superior Politécnica de Chimborazo (ESPOCH), Riobamba, 060155, Ecuador.

Abstract:

Miniaturization trends and rapid advancements in the medical device industry have made it possible for everyone's physiological signals and routine behaviors to be monitored conspicuously and ubiquitously, without anyone even realizing its happening. Energy efficiency is one of the most important and hotly contested topics in healthcare because of the limited power of traditional wearable sensors while sensing. In this research, the Texas Instruments Analog-Front-End (AFE) chip type ADS1292R is used to create a wearable, wireless Electrocardiogram (ECG) tracking solution relying on a single chip. The developed chip records real-time ECG data on 2 chosen channels to continually monitor each person's heart activity. These four components make up a Right-Leg-Drive (RLD) circuit: two channels, an AFE, a lead-off sensor, and a medical screening signal. The empirical design took into account 60 hertz of background noise and human ECG data obtained at speeds ranging from 60 to 120 beats per minute (BPM). Finally, many standard TPC algorithms are compared with a suggested "Adaptive Energy-Efficient Transmission Power Control" (AETPC) algorithm. The empirical results show that the designed device efficiently gathers ECG data in real-time and that the suggested AETPC algorithm saves 35.5% more energy than traditional TPC while having a little larger Packet-Loss-Ratio (PLR).

Keywords: Healthcare, ECG data, Wearable, Adaptive Energy-Efficient Transmission Power Control (AETPC)

DOI: [10.24297/j.cims.2023.20](https://doi.org/10.24297/j.cims.2023.20)

1. Introduction

Traditional communication networks that were largely created for applications focused on human beings are experiencing enormous issues as wearable devices grow more integrated into our daily lives. Fifth-generation (5G) wireless networks are expected to enable new levels of high capacity, low latency, and widespread connectivity. The main difficulties that wearable

communication devices face are discussed in this paper. Device-to-device (D2D) communication, software-defined networks (SDN), cloud/edge technologies, and cloud radio access networks (CRAN) are all combined in cloud/edge communication architecture. With the help of this multilayer communications architecture, compute offloading is possible. This enables the transfer of computationally demanding and latency-sensitive applications to adjacent edge nodes via cellular or other wireless technologies, or to close-by devices via D2D communications (Sun et al., 2018). It has been suggested that there are problems with processing and analyzing data from wearable devices as well as traditional cardiovascular diagnostic tests. Deep learning-based automatic classification and diagnosis of aided ECG signals for COVID-19 patients is an effective solution to these issues. The introduction of 5G has also made it possible to process a sizable volume of monitoring data using a solution that has high throughput and low latency. Several open source platforms, like Ignite, Geode, and Spark streaming, have been developed as a result of the development of big data technologies and allow for the real-time analysis of operational data. Because this area of study is constantly getting better, artificial intelligence is being used more and more frequently in medical diagnostics. Deep neural networks (DNN) have become frequently utilized in automatic ECG diagnosis in recent years to meet the demands of high-speed and high-precision ECG analysis (Tan et al., 2021). Edge computing connects military organizations to wearable computing devices on the battlefield, improving, securing, and raising troop decision-making accuracy. Along with all of this, edge computing's scalability, flexibility, and dependability make it a desirable substitute for military automation on a global scale. According to projections, the fifth generation of cellular network technology will have ten times more capacity than the legacy network that is now in use (5G). The goal of 5G is to link digital devices that require a lot of data to operate automatically, not only to increase network speed. Most major 5G applications will primarily target the military rather than the general population (Sharma et al (2020). To fuel the Internet of Things, 5G wireless communication technology is anticipated (IoT). They provide methods for incorporating wireless cloud platforms for dense cooperative signal and information processing, taking into account the rapidly expanding IoT device market (WCN). They give a summary of the WCN architecture and the cloud characteristics that go along with it, ranging from distributed synchronization and sensing to cooperative networking. For crucial process monitoring, the 5G evolution provides a multi-Radio Access Technology (RAT) architecture, in which the WCN nodes connect to the current field equipment using a wireless Industrial Internet of Things (IIoT) standard (Soatti et al (2019). The 5G and 6G communications, as well as other emerging developments, including new services, will address the recent

revolution in smart wearables and wireless devices. Smart wearables are useful in many aspects of daily life, such as healthcare, entertainment, and search and rescue. The wearables of the future typically blend inconspicuously and discretely with clothing. Because they are often constructed on stiff substrates, antennas in systems for on-body applications have proven difficult. The user's ability to interact with some electronic gadgets can be expanded, though, by integrating antennae into clothing. The task of designing textile antennas is difficult because the materials' properties influence the antenna behavior and because fabrics are very flexible and compressible (Loss et al. (2020)).

The following describes the paper's contribution:

1. We created the "Adaptive Energy-Efficient Transmission Power Control (AETPC) algorithm" to enable 5G for wearable technology and human-computer interfaces.
2. A wearable, wireless Electrocardiogram (ECG) tracking system dependent on a single chip is created using the Texas Instruments Analog-Front-End (AFE) chip type ADS1292R.

The sections of this paper are listed below: Section II provides a list of pertinent works and a description of the issue, Section III presents materials and methods, Section IV discusses the suggested strategy of adaptive energy-efficient transmission power control, and Section V presents performance analysis, and Section VI concludes the investigation.

2. Related Works

Alrashid and Nasri (2021) presented research on innovative wireless technology created for "Wireless Body Area Sensor Networks," solving signal conditioning concerns, bandwidth allocation, safety, and upcoming research problems (WBASN). Wearable technology presents a potent new tool because of medical services, surgical rehabilitation services, and IoT systems. In addition to monitoring body heat, heart rate, pulse rate, higher blood pressure, electro-dermal activity, as well as other health indicators, a wireless body-area network can also record electrocardiograms. Wearable gadgets use radio frequency identification (RFID) technology and electronics. RFID antennas and technology are discussed in (Sabban, A., 2020).

Anline and Gomathy (2021) examined the design and communication methods for e-health systems that permit continuous smart monitoring via 5G. The architecture of the 5G network is also apparent. By going above and above the necessary properties of high throughput, hyper latency, high population density, hyper-dependability, and superior energy efficiency, emerging 5G networks significantly improve smart healthcare coverage.

Varsie et al. (2020) evaluated the requirements of the use cases stated in the NR-REDCAP 3GPP Study Item of Release 17—such as wearables, industrial IoT, and video surveillance—with the restrictions of such capabilities. It also discusses the difficulties of creating a new air interface for 5G devices with constrained sub-6 GHz band capabilities as well as the crucial enablers needed to meet those use case requirements. 5G will overcome this problem even with the continued usage of an energy-intensive Ultra-Dense Network (UDN).

Slalmi et al. (2020) created a New Radio Access that uses an energy-efficient Call Admission Control (CAC) modeling technique for the Internet of Things (IoT) (NR 5G).

Jin et al. (2022) examined the shortcomings of wearable technology and considered how edge computing could help to mitigate these shortcomings. They then thoroughly assess earlier studies from four perspectives: computation scheduling, information perception, energy conservation, and security.

Heidari et al. (2021) suggested that different power harvesting and management techniques at the circuit, device, and system levels will be the most important component of IoT devices. The self-power and sustainability of IoT devices in the 5G network should be a top priority for the electronics and communications sectors.

Dananjayan and Raj (2021) proposed that wearables with trustworthy sensors and a 5G network can be utilized to remotely monitor patients. Virtual patient consultations, augmented reality (AR) and virtual reality (VR)-based simulated surgeries, robotic surgeries powered by artificial intelligence (AI), real-time maintenance of ambulances and other medical devices, and dynamic huge data repositories are additional applications for 5G technologies in the healthcare industry. To help designers create a device that can be used in the health care business with 5G technology along with upcoming 6G wireless networks, a critical analysis of medical equipment and the many optimization techniques used is offered (Kouhalvandi et al. (2022)).

Wang et al. (2022) started by looking at the frameworks currently in place for wearable device applications in 5G telemedicine and identified current difficulties. Then, using 5G mobile edge computing (MEC), they presented a multi-layer telemedicine model that dynamically links wearable technology with the Open electronic medical records system (EMR).

3. Material And Methods

A) Wearable ECG Collection Platform

This effort created a wearable ECG and breathing system on a single chip using a Texas Technologies "Analogue Front End" (AFE) chip type ADS1292R. There are numerous channels on this chip, notably ones for real-time continuous Electrocardiography and continuous-time breathing monitoring. A circuit diagram of the semiconductor ADS1292R is shown in Figure 1. The ADS1292R processor's wearable upgrades included two bitmap delta-sigma ADCs (Analog-to-Digital converters) with variable boosting amps and collection levels ranging from 1 to 12. The ADCs were configured with a carrier frequency range of 125 to 8000 samples per second (SPS). Digital data was managed by an SPI link, or serial peripheral interface.

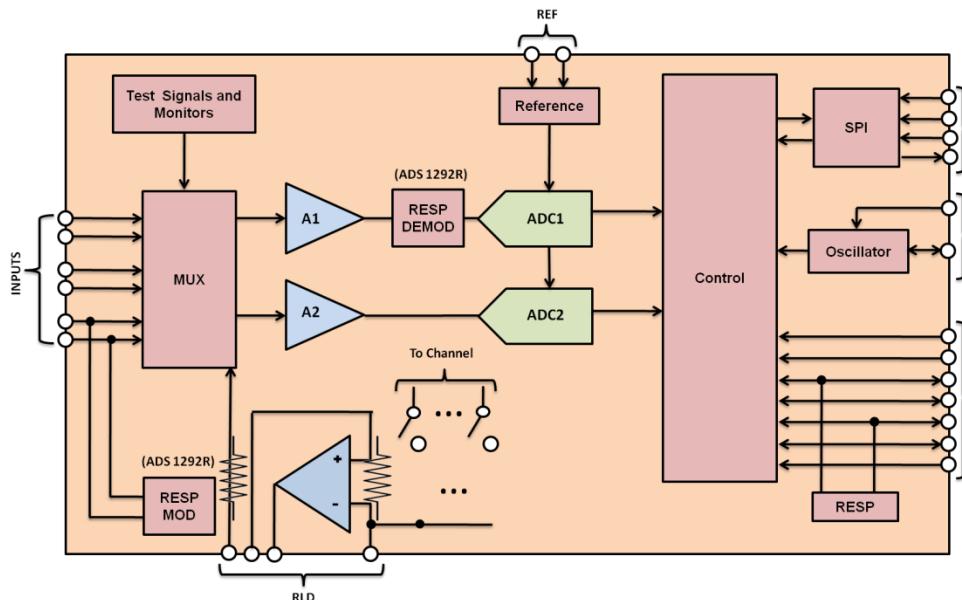


Figure 1: The ADS1292R chip's block diagram.

Figure 2 uses a typical Holter that has three connected leads and one lead (E1-E3) points to demonstrate to the intended wearable system measures ECG.

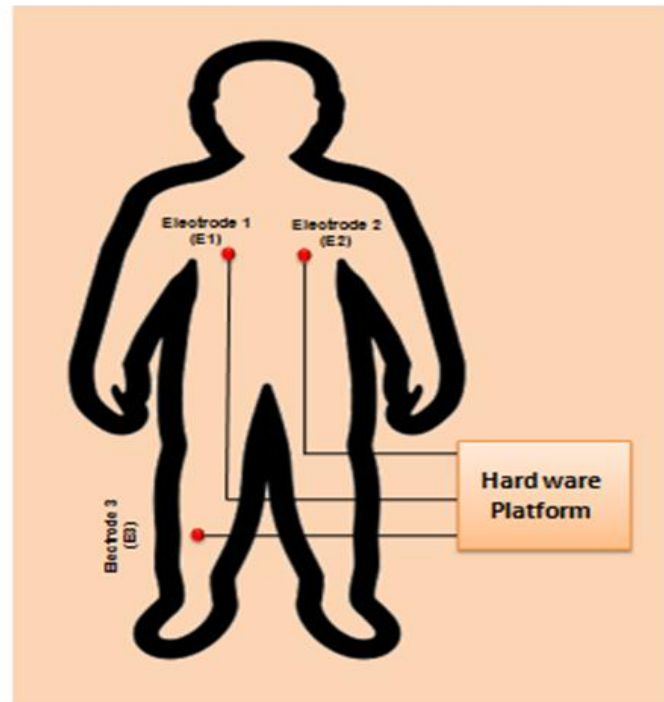


Figure 2: Measuring electrocardiograms (ECGs) using a single lead standard Holter

The leads that were discovered were near the cardiac axis. This efficient and exact method generates a high-quality ECG signal with improved performance in clinical activities when the cardiac axis is modified appropriately and the site is chosen. The positioning of the cardiac axis and lead selection allows for a transparent inspection and diagnosis as well as the transfer of useful information. Ag/AgCl electrodes are used in the experimental design of this study to capture and record the signals of human vital signs. On our test bed, a third reference electrode was placed 10 cm away in the lower-left corner, and two electrodes were placed on the surface of the chest extremely close to the heart. With a greater R-peak amplitude and QRS-complex waves, such a design produces ECG signals that are neater, cleaner, and more effective. The created wearable gadget had metal buttons on one side that connected it to the other side and was fastened to the skin on the other. Other academics have also been developing hardware-based platforms for the use of wearable technology to acquire ECG data to set up investigations. Additional details regarding the created ECG equipment are provided in Table 1, including its multiple methods, the necessary power, and the battery type.

Table 1: Numerous techniques exist for utilizing energy.

Methods	Energy consumption	cell
Leadoff detected	Lowest 14.4 NW, Highest 52.8 μ W	80% of power is saved as compared to the conventional

		batteries
Standby	160 μ W overall consumption, and Low Power: 335 μ W/channel	Coin cell battery
Acquisition of Noise ECG	42 mW	Ten-year battery lifetime in the absence of system power

B) Electrocardiogram Data Filtration

A high-pass filter (HPF) with a cutoff frequency of 0.67 Hz and a low-pass filter (LPF) with a cutoff frequency of 60 Hz was used to produce three filters that successfully remove noise from ECG data (cutoff frequency 100 Hz). The biquade direct form transposed-II algorithm and the bilinear transformation method were used to create the filters.

This psychology indicates that wearable technology collects from the human body typically contains some extra undesired noise. Therefore, it is essential to remove that unwanted information from biosignals to acquire unambiguous signals for use in subsequent healthcare applications. The hardware platform cannot completely filter out all of the sounds that can disrupt biomedical engineering obtained from the human body. To exclude irrelevant data from the first acquired signals from wearable devices, it is vital to utilize the appropriate filters. The key constraint for completely filtering noisy information, capacitors, are used in the design of hardware filters; as a result, the justification of hardware filters is not fully addressed from the points of view of both effective construction and high visibility (figure 3).

They are frequently essential to code filtration since they allow for the precise control of clipped frequencies. Due to the relatively low signal levels, filtering is required to eliminate a variety of undesired noise signals (1 mV for biomedical engineering like the ECG). The uneven effect size between the electrode and the human body, electrical instrument noise in the environment, power-line (50/60 Hz), muscle noise, and internal noise during the production of wearable ECG devices are the most frequent causes of noise in the ECG signal. In this section, it was explained that since heart rate data is delicate, it is crucial to remove power line noise before sending it to the computer that will be used to communicate with the end user.

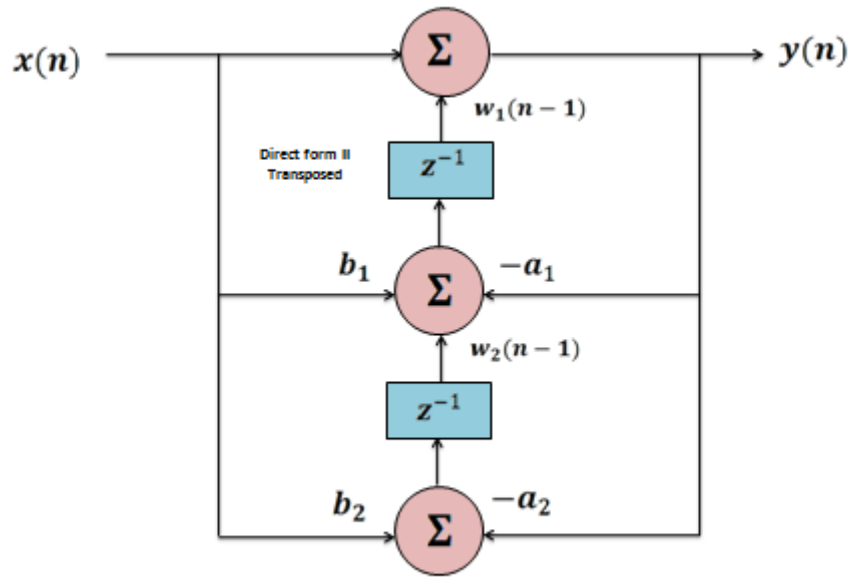


Figure 3: Block schematic for Biquade Direct Form Transposed-II

While X_i and X_j at time s , represent the samples in outlets i and j . This can also be considered while analyzing the $Y, X(s)$, as well as $Y(s)$, are the input and output, respectively. The filter's A_i and B_j (which may vary for every outlet), and K_i (a collection of interesting factors) parameters in equation (1).

$$K = \tan(\pi \times \omega) \tag{1}$$

Therefore, w is a constant $p_i(\pi)$ number of 3.141592653 that represents a normalized cut-off frequency in equation (2).

$$\begin{aligned} norm &= \frac{1}{\left(1 + \frac{K}{Q} + K \times K\right)} \\ a_0 &= (1 + K \times K) \times norm \\ a_1 &= 2 \times (k \times K - 1) \times norm \end{aligned} \tag{2}$$

The filter coefficients calculated throughout the filtration duration are a_1 and b_1 . Similar to the output signal $Y(s)$ was multiplied by a_1 and a_2 . b_0 as well as b_2 are represented as the feed-forward coefficients and are said to multiply the input signal $X(s)$ in equation (3).

$$b_2 = \left(1 - \frac{K}{Q} + K \times K\right) \times norm \tag{3}$$

Q , a quality element has a value of 0.707 in this equation above. As depicted in Figure 3, The MCU's method is linearly transposed twice, as seen in equations (4)-(7).

$$\frac{Y(z)}{X(z)} = \frac{b_0 + b_1 z^{-1} + b_2 z^{-2}}{1 + a_1 z^{-1} + a_2 z^{-2}} \quad (4)$$

$$Y(n) = b_0 x(n) + \omega_1(n-1) \quad (5)$$

$$\omega_2(n) = b_1 x(n) - a_1 y(n) + \omega_2(n-1) \quad (6)$$

$$\omega_1(n) = b_2 x(n) - a_2 y(n) \quad (7)$$

4. Proposed Adaptive Energy-Efficient Algorithm

A. Database description

USC-HAD: Data from 12 daily activities performed by 14 participants are included in the USC-HAD dataset. A motion node that was securely mounted on the subject's right hip was used to record the data as they were instructed to walk however they saw fit such as forward, upstairs, etc. Three 3-axis sensors—a 3-axis accelerometer, 3-axis gyroscope, and 3-axis magnetometer—combine to form the motion node. 100 Hz continues to be the highest sampling frequency (Singh et al, 2020). Table 2 offers an overview of the information along with citations to the pertinent sources.

Table 2: The data set used in experimental and validation research projects

Database	Location and type of sensor	Sampling freq	# volunteers	Sensor placement	# Activities
USC-HAD	Motion node	100 HZ	15	The subject's right up had a motion node tied to it using a cellphone.	Walking, jumping, napping, and using the elevator are among the ten physical activities.

B. Adaptive Energy-Efficient Algorithm

To transmit ECG data across a hardware and software platform, they advise using the adaptive energy-efficient transmission power control (AETPC) technique, which they also analyze. Transmission power fluctuates due to base station demand (BS) estimates and the dynamic wireless channel (TP). In contrast to AETPC, which is only useful in dynamic situations, a modification of the adaptive power control method is proposed. While AETPC can be used in both static and dynamic situations, there are differences in the power distribution methods for each. The traditional TPC methods, such as Gao's, constant TPC, and Xiao's methods, are also

contrasted with the proposed AETPC because they ineffectively follow the characteristics and, as a result, either forego efficiency savings or channel reliability. The majority of the energy is used in control packets and delivering feedback and acknowledge (ACK) information when power management algorithms are built using standard methods, such as those proposed by Gao and Xiao, which do not account for all channel characteristics.

Constant TPC provides linear direct high power, however, this is not practical because it either decreases energy efficiency or dependability. The primary experimental parameters are the estimated average of the RSSI samples (RSSI average, R_{Lowest}) which is preferred after the most recent RSSI sample is lost or dropped at the start of the first transmission; The strengths are the 2 dbm difference in average weight between a better channel (one with a high RSSI and minimal packet drop) and a bad channel (one with a low RSSI and large packet drop). Both the variable upper threshold and the average weight of a good channel are 83 dBm. R Goal (85 dbm) has a little lower RSSI than RSSI objective in terms of packet loss (85 dbm). To determine and, respectively, meet the user's best transmission power level and requirement, AETPC uses an adaptive on-demand technique (8)-(9).

$$\bar{R} = R_{lowest} + (1 - \alpha_1) \times \bar{R} \quad (8)$$

$$\bar{R} = R_{lowest} + (1 - \alpha_2) \times \bar{R} \quad (9)$$

Here, ΔP indicates the maximum transmission level change and is modified in equation (10) in line with the demand of RSSI and variation in the wireless channel.

$$\Delta P = \begin{cases} 2 & \text{if } \bar{R} < TRL \\ -1 & \text{if } \bar{R} > TRH_{var} \\ 0 & \text{if } TRL < \bar{R} < TRH_{var} \end{cases} \quad (10)$$

Where and are, respectively in equation (11), (12), the standard deviation in σ dbm along with the n number of RSSI samples.

$$TRH_{var} = TRL + \sigma \quad (11)$$

$$\sigma = \sqrt{\frac{1}{n} \sum_{i=1}^n (R_i - \bar{R})^2}, i = 1, 2, \dots, n \quad (12)$$

When transmission power is spread fairly, communication is more reliable and long-lasting. The lowest RSSI R_{Lowest} is one of the essential components since it guarantees uninterrupted

communication between the transmitter and BS nodes. Data transport is hampered and the transmission rate is substantially reduced if it is lost. By employing fixed RSSI threshold values, traditional constant TPC and other approaches, including those of Gao and Xiao, inadequately take into account the dynamic character of the wireless interface. They suggested that uplink data is provided linearly as required and that the transmitter node and the BS are both monitoring the proposed energy-efficient transmission power control (ETPC). The next TP level is chosen and distributed by BS using the average RSSI (\bar{R}) of all data samples.

Algorithm 1: Pseudocode for the energy-efficient power control

Rlatest: (RSSI of recent samples)

Rlowest: (Samples received after the most recent sample's RSSI)

Rtarget: (RSSI average value):(RSSI target)

Stage 1: if Rlatest > \bar{R}

Stage 2: $\bar{R} = R_{\text{lowest}} + (1 - \alpha_1) \times \bar{R}$

Stage 3: else Rlatest < \bar{R}

Stage 4: $\bar{R} = R_{\text{lowest}} + (1 - \alpha_2) \times \bar{R}$

Stage 5: end if

Stage 6: $\bar{R} > TRH_{\text{var}}$

Stage 7: $\Delta p = \begin{cases} 2 & \text{if } \bar{R} < TRL \\ -1 & \text{if } \bar{R} > TRH_{\text{var}} \\ 0 & \text{if } TRL < \bar{R} > TRH_{\text{var}} \end{cases}$

Stage 8: else if { $\bar{R} < TRH_{\text{var}}$ }

Stage 9: $\Delta p = \begin{cases} 2 & \text{if } \bar{R} < TRL \\ -1 & \text{if } \bar{R} > TRH_{\text{var}} \\ 0 & \text{if } TRL < \bar{R} > TRH_{\text{var}} \end{cases}$

Stage 10: else { $TRL \leq \bar{R} \leq TRH_{\text{var}}$ }

Stage 11: avoiding action

Stage 12: end

The proposed pseudocode for the ETPC approach is shown in Figure 4. The four distinct types of thresholds (RSSI) are fixed lower threshold (TLL), variable higher threshold (TRH var), and received signal strength indication.

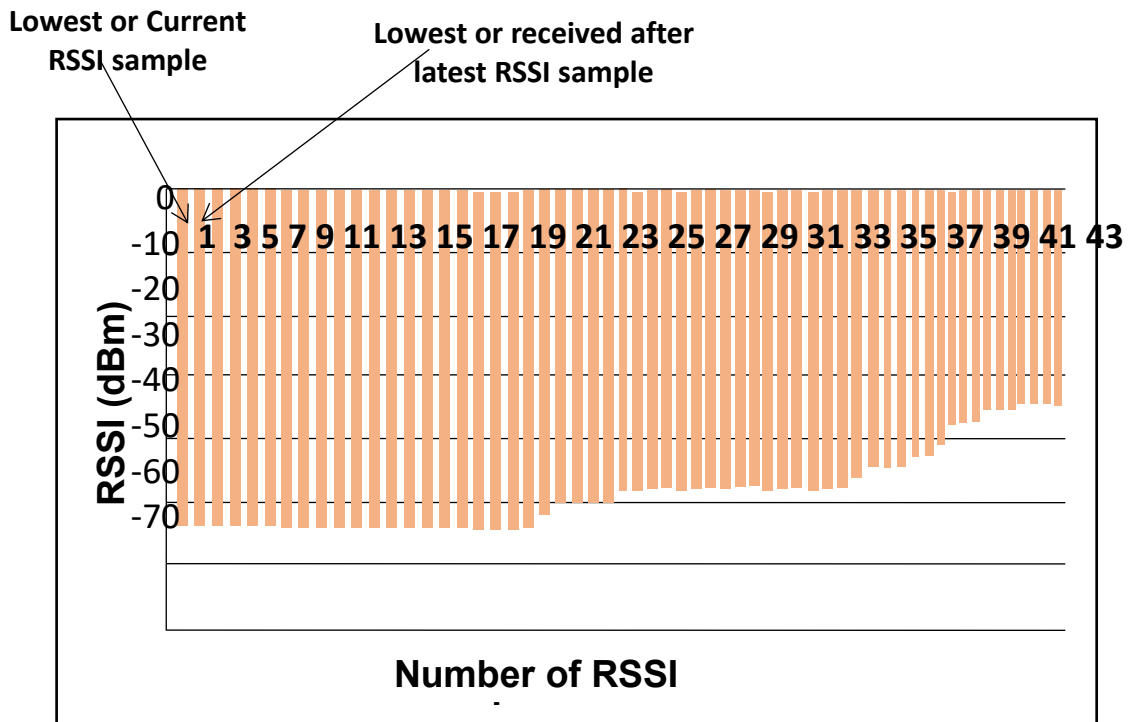


Figure 4: samples of RSSI data are transmitted

5. Experimental Results And Discussion

In our trial, thirty healthy participants participated. To test the patients, the room temperature was kept between 21 and 26 °C from 9:00 am to 4:00 pm. This section examines the effects of various power line noise filters on the functionality of a wearable platform with a single chip for monitoring ECG signals. The three different filter types' potency was evaluated while rectifying the ECG signal. Through a full experimental setup on a platform with integrated hardware and software, the suggested AETPC and the standard transmission power regulation were also contrasted while accounting for combined RSSI along with the value of transmission power. The human body's heart rate (HR) was measured in experiments both at rest and while pedaling a bicycle. Participants' heart rates rise when using the bike; when they are not using the bike, their heart rates gradually return to normal. Human ECG data, which can produce a variety of noise, comprising baseline wandering, cabling noise, and AC power line noise, was used to evaluate the HR algorithm. When a person was steering or peddling a bike, the human body generated the ECG signal that was employed in our experiment. Using an ECG simulator, the signal was confirmed and other types of noise were produced. The initial prototype ECG signal was first shown on a computer before the ECG device wirelessly transmitted raw data, which was afterward acquired via a Bluetooth Low Energy (BLE) dongle device connected to the PC (PC). A computer program analyses the ECG after it has been filtered and displayed. The adopted ECG

simulator from Fluke, the "Fluke Biomedical 215A Patient Simulator," likewise generates a variety of signal artifacts. Since they used common electrodes rather than health electrodes for the prototype, the final product will be 4 cm by 4 cm smaller than the prototype, which was 6 cm by 12 cm in size. They made use of our custom-made wearable ECG equipment and the chest-to-right hip experimental setup. The resulting real-time ECG data was filtered to remove power-line noise and artifacts using hardware notch, HPF, and LPF. The results of these apps were compared. To compare the energy efficiency of our new AETPC algorithm to that of traditional TPC techniques, average transmit power (AVG TP) was employed. The outcomes demonstrated a 35.5% gain in energy efficiency using the proposed AETPC algorithm. Additionally, it was discovered that the continuous TPC technique was inefficient because it either consumed more energy when the channel condition was favorable or decreased dependability when it was unfavorable. Additionally, dynamic channel statuses could not be changed.

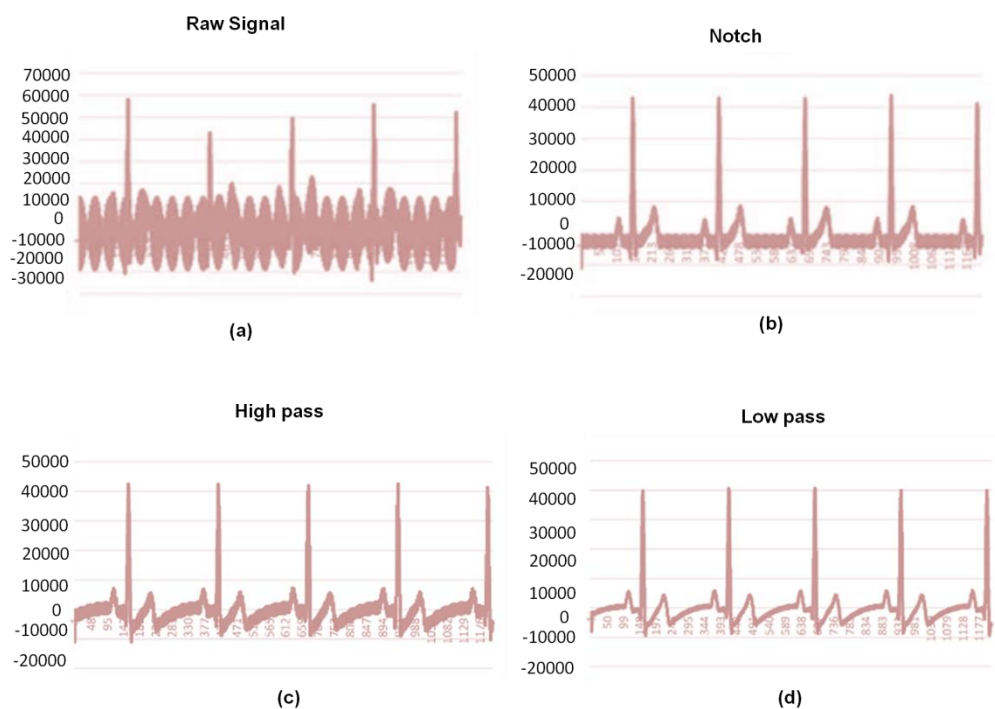


Figure 9

Figure 5: Filtering ECG data at 60 BPM with 60 Hz noise using a notch filter, HPF and LPF

Figure 5 displays the human electrocardiogram signal at a noise level of 60 Hz and 60 beats per minute (BPM). The unfiltered ECG signal and the signals that have undergone notch, HPF, and LPF are shown in Figures 5a–5d. Each peak ought to occur in a second because the BPM was 60. 161 and 410, respectively, have been recognized as the first and second peaks computing the

various results in 250. Since our rating was 250 samples per second (SPS), they can compute 250 SPS by multiplying 1 by 250. The two peaks are at 157 and 412 with a notch filter applied a differential of 255, and a sample rate of 255 SPS.

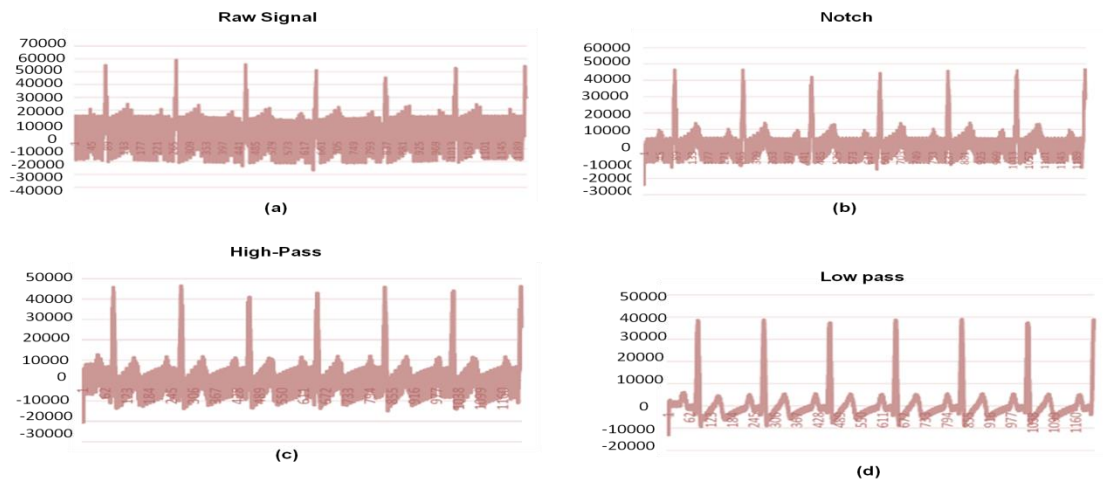


Figure 10

Figure 6: Filtering of ECG data at 50 Hz noise and 80 BPM. Examples of filters include raw data, notch filter, HPF, and LPF

Figure 6 represents the human Electrocardiogram data with a noise level of 50 Hz and 80 bpm. In contrast to Figures 6b–6d, which show the filtered data after applying notch, HPF, and LPF, respectively, it shows the raw Electrocardiogram signals without any filter procedures. It was discovered that the LPF outperformed the notch and HPF and that the notch filter was less effective at reducing noise than the HPF. Consequently, the LPF can be used to clean up real-time heart rate variability data by removing artifacts and power-line noise.

Figure 7 shows the human ECG data at a noise level of 50 Hz and 120 BPM. Figures 7b–7d show the filtered data after applying notch, HPF, and LPF, while Figure 11a displays, raw data without any sort of filtration. When it came to noise-filtering, they discovered that the HPF functioned better than the notch filter and the low-pass filter. The LPF is therefore a useful technique for removing artifacts and power-line noise from heart rate variability data in real-time.

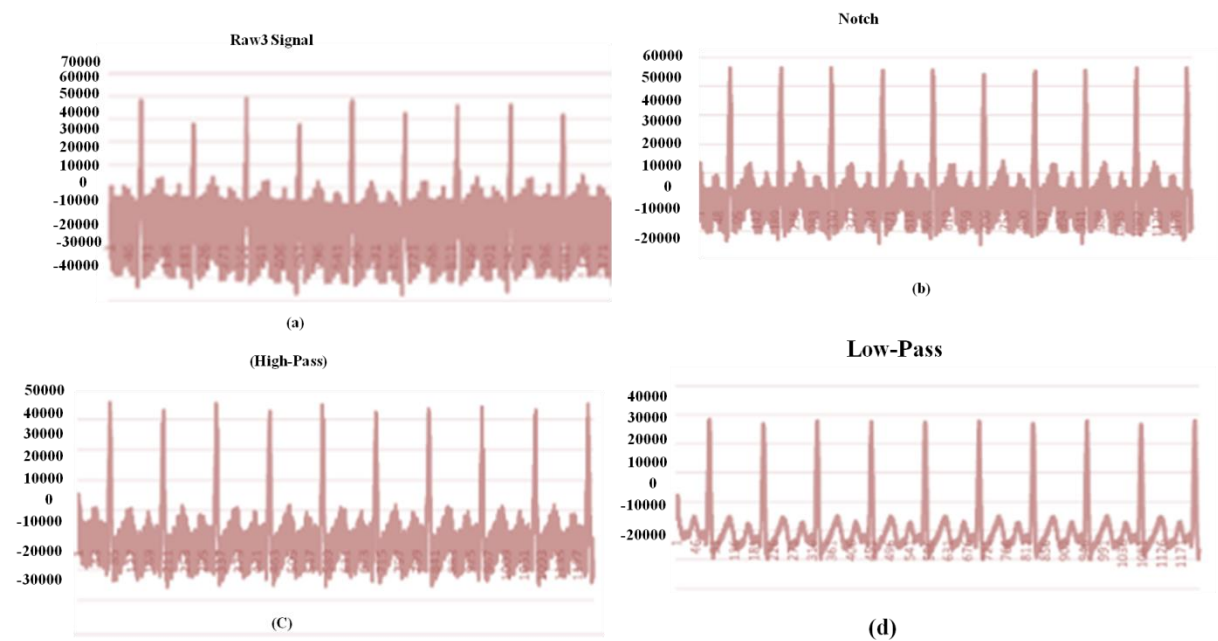


Figure 7: Filters that can be used to filter raw ECG data at 120 BPM and 50 Hz noise

Figure 8 shows the outcomes of an ECG performed on a human subject at a noise level of 50 Hz and 180 BPM. Figures 8b–8d shows the filtered data after applying notch, HPF, and LPF. Figure 8a shows the raw data that has not been filtered. They found that the (LPF) performed better than the notch filter along with the notch filter had lower effectiveness for removing noise. As a result, the LPF is a helpful method for reducing artifacts and power-line noise from real-time heart rate variability data.

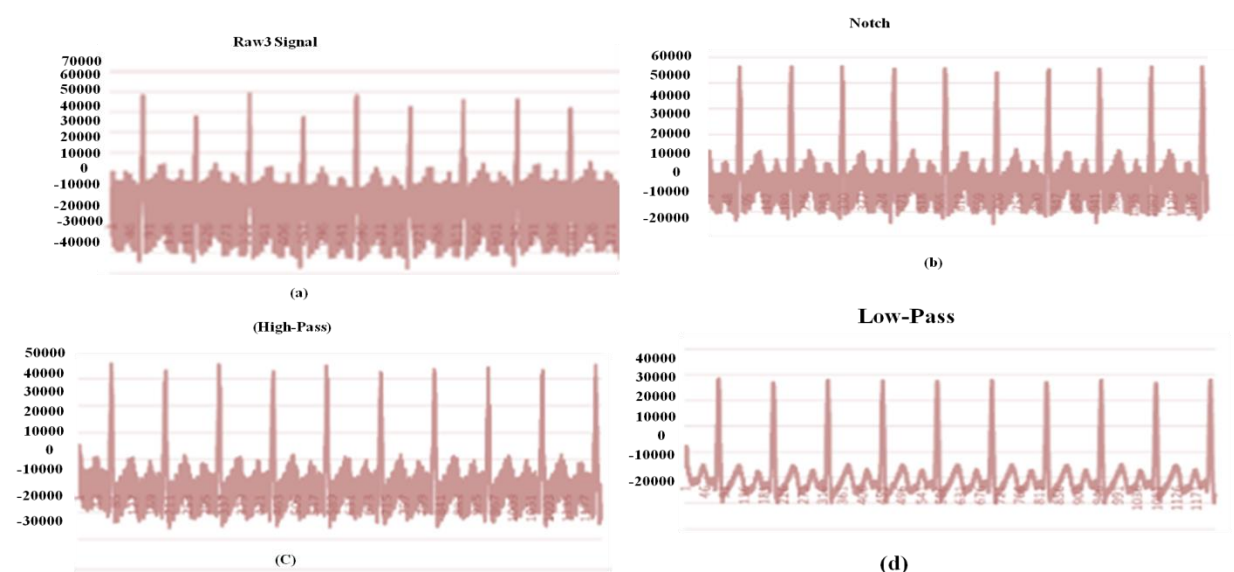


Figure 8: Filtering of ECG data at 50 Hz noise and 180 BPM. The filters shown are raw data, a notch filter, HPF, and LPF

In conclusion, the noise was removed from real-time ECG data at 80, 120, and 160 beats per minute utilizing the notch, HPF, and LPF. The ECG signal was shown to degrade more at higher BPM values and less at lower BPM values. As shown in Figures 5, 6, 7, and 8, the HPF reduced power-line noise levels more effectively than the notch filter and artifacts, while the LPF outperformed the other filters.

A. RSSI

An RSSI that was closer to 0 is stronger, and one that is closer to -100 is weaker. We want your RSSI to be as high as it can be for optimum results. We won't likely experience strong Wi-Fi bandwidth performance if the RSSI is less than -70 dBm, according to a helpful rule of thumb. Outperforming the outcomes for the currently used methods of H-LSTM (55dbm), MET (70 dbm), and GDMM (89 dbm), the proposed strategy obtained 96 dbm. RSSI demonstrates the suggested system's excellent performance. Figure 9 depicts a comparative analysis of RSSI values.

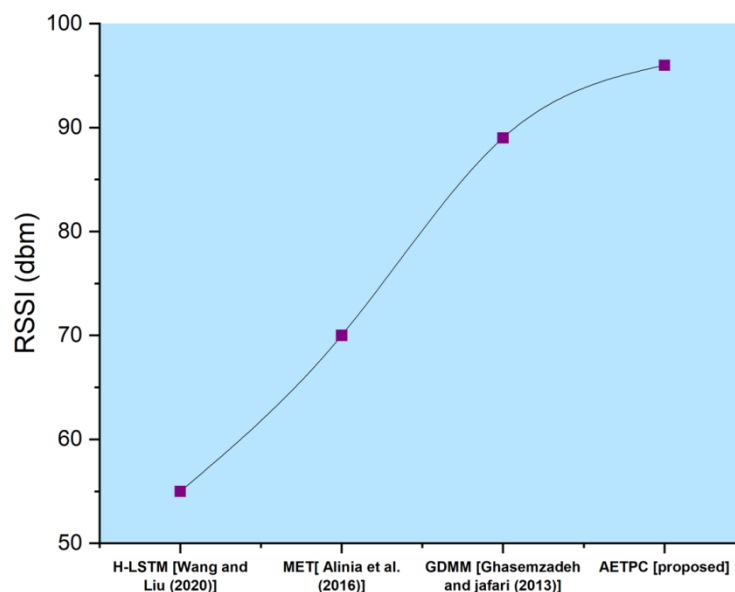


Figure 9: Comparative Analysis of RSSI

B. Processing time

The processing times indicate how long it normally takes us to process an application. A processing period begins the day we receive an application and concludes when we make a choice. The proposed strategy (AETPC) obtained 60 secs, outperforming the results for the

already employed methods of H-LSTM (97 secs), MET (80 secs), and GDMM (72 secs). Processing time displays the subpar performance of the proposed system. Comparative processing time analysis is shown in Figure 10.

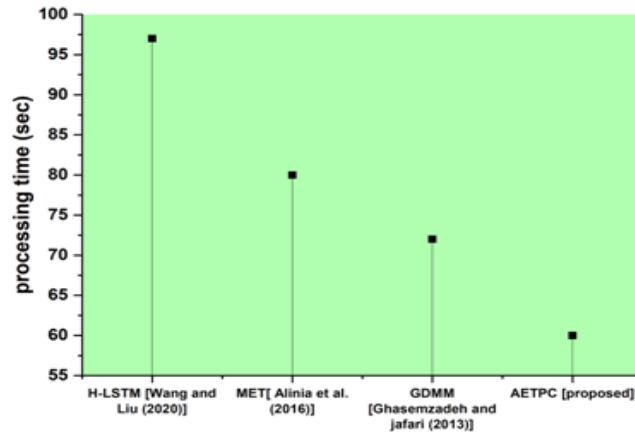


Figure 10: Comparative analysis of processing time

C. Transmit power

The relationship between an access point radio's transmit power and effective range is inverse. A signal's transmit power determines how far it can travel and how many obstructions it can pass through. The relationship between an access point radio's transmit power and effective range is inverse. A signal's transmit power determines how far it can travel and how many obstructions it can pass through. The proposed technique (AETPC) achieved 96 dbm in comparison to the results for the previously employed methods of H-LSTM (62 dbm), MET (78 dbm), and GDMM (84 dbm). Transmit power demonstrates the proposed system's improved performance. Figure 11 displays a comparative examination of transmit power.

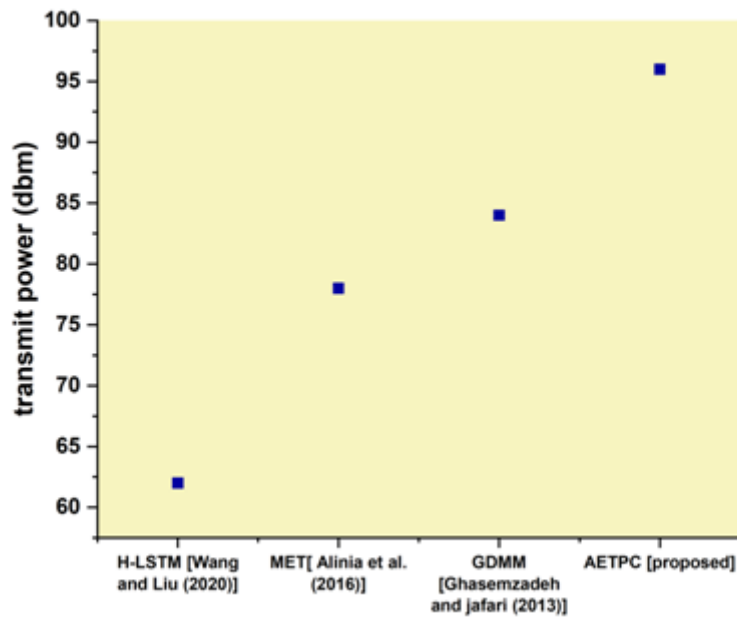


Figure 11: Comparative analysis of transmit power

D. System efficiency

In electronics and electrical engineering, a system's efficiency is calculated by dividing its useable power output by the entire amount of electrical power it uses (a fractional expression), and is commonly represented by the Greek minuscule letter eta. The proposed strategy (AETPC) attained 97% in comparison to the results for the previously employed methods of H-LSTM (68%), MET (75%), and GDMM (88%). System efficiency displays the enhanced performance of the suggested system. An analysis of system effectiveness in comparison is shown in Figure 12.

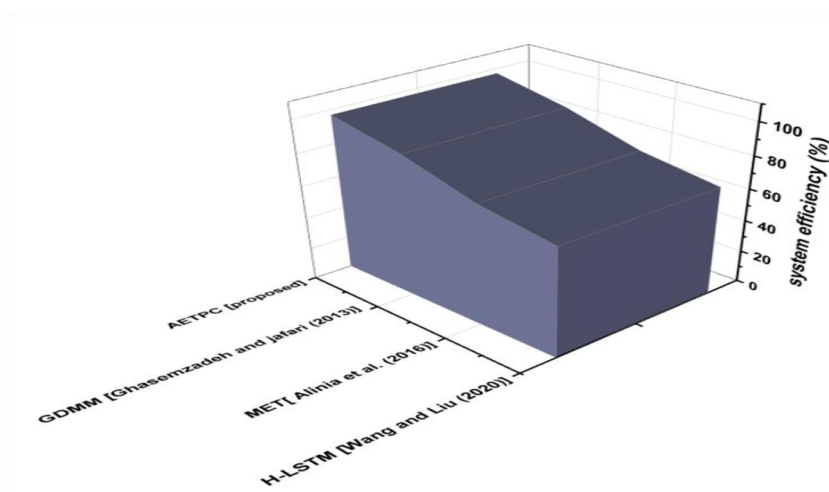


Figure 12: Comparative analysis of system efficiency

6. Discussion

For sensing and signal processing, the AETPC algorithm is used in wearables and other man-machine interfaces that support 5G. Long-short hybrid memory (H-LSTM) It is difficult to apply the dropout method to solve the overfitting issue with LSTM. Dropout is a regularization technique that probabilistically excludes input and recurrent connections from weight and activation updates when training a network. Limitations of using the metabolic equivalent of task (MET) to gauge the intensity of physical activity or exercise. Not every MET is made equally. In other words, not all MET offer the same advantages for health. It is not possible to extract data with the same high resolution from high-frequency bands since the wavelet transforms at every stage of signal breakdown, only low-frequency bands are broken down. As a result, our suggested solution outperforms current methods.

7. Conclusion

Everyone is experimenting with wearable technologies for smart healthcare, with a particular focus on ubiquitous or pervasive sensing. However, their main problem with energy use always keeps them from performing to their fullest ability. A wearable wireless electrocardiogram (ECG) monitoring system for medical purposes is developed in this study using the analog front end (AFE) chip model ADS1292R. The human behavior that is being captured by current datasets is not complete. For the research on AETPC, we'll use a larger, more diverse dataset to get a high level of recognition accuracy. Our test findings confirm the proposed architecture's potency in lowering the system's energy usage.

Reference

1. Sun, H., Zhang, Z., Hu, R.Q. and Qian, Y., 2018. Wearable communications in 5G: Challenges and enabling technologies. *IEEE vehicular technology magazine*, 13(3), pp.100-109.
2. Tan, L., Yu, K., Bashir, A.K., Cheng, X., Ming, F., Zhao, L., and Zhou, X., 2021. Toward real-time and efficient cardiovascular monitoring for COVID-19 patients by 5G-enabled wearable medical devices: a deep learning approach. *Neural Computing and Applications*, pp.1-14.
3. Sharma, P.K., Park, J., Park, J.H. and Cho, K., 2020. Wearable computing for defense automation: Opportunities and challenges in 5G network. *IEEE Access*, 8, pp.65993-66002.

4. Soatti, G., Savazzi, S., Nicoli, M., Alvarez, M.A., Kianoush, S., Rampa, V. and Spagnolini, U., 2019. Distributed signal processing for dense 5G IoT platforms: Networking, synchronization, interference detection, and radio sense. *Ad Hoc Networks*, 89, pp.9-21.
5. Loss, C., Silveira, T.M., Pinho, P., Salvado, R. and de Carvalho, N.B., 2020, July. Design and Analysis of the Reproducibility of Wearable Textile Antennas. In *2020 12th International Symposium on Communication Systems, Networks and Digital Signal Processing (CSNDSP)* (pp. 1-5). IEEE.
6. ALRASHIDI, M. and NASRI, N., 2021. Wireless body area sensor networks for wearable health monitoring: technology trends and future research opportunities. *International Journal of Advanced Computer Science and Applications*, 12(4).
7. Sabban, A., 2020. Wearable Technologies for 5G, Medical and Sports Applications. In *Wearable Systems and Antennas Technologies for 5G, IoT and Medical Systems* (pp. 263-288). CRC Press.
8. Anline Lizie, R. and Gomathy, C., 2021. A Review of Design and Protocol for Smart Continuous Monitoring E-Health Systems in 5G. *Advances in Automation, Signal Processing, Instrumentation, and Control*, pp.467-475.
9. Varsier, N., Dufrène, L.A., Dumay, M., Lampin, Q. and Schwoerer, J., 2021. A 5G New Radio for Balanced and Mixed IoT Use Cases: Challenges and Key Enablers in FR1 Band. *IEEE Communications Magazine*, 59(4), pp.82-87.
10. Slalmi, A., Kharraz, H., Saadane, R., Hasna, C., Chehri, A. and Jeon, G., 2019, November. The energy efficiency proposal for IoT calls for admission control in the 5G network. In *2019 15th International Conference on Signal-Image Technology & Internet-Based Systems (SITIS)* (pp. 396-403). IEEE.
11. Jin, X., Li, L., Dang, F., Chen, X. and Liu, Y., 2022. A survey on edge computing for wearable technology. *Digital Signal Processing*, 125, p.103146.
12. Heidari, H., Onireti, O., Das, R. and Imran, M., 2021. Energy harvesting and power management for IoT devices in the 5G era. *IEEE Communications Magazine*, 59(9), pp.91-97.
13. Dananjayan, S. and Raj, G.M., 2021. 5G in healthcare: how fast will the transformation?. *Irish Journal of Medical Science (1971-)*, 190(2), pp.497-501.
14. Kouhalvandi, L., Matekovits, L. and Peter, I., 2022. Magic of 5G Technology and Optimization Methods Applied to Biomedical Devices: A Survey. *Applied Sciences*, 12(14), p.7096.

15. Wang, Y., Tran, P. and Wojtusiak, J., 2022. From Wearable Device to OpenEMR: 5G Edge Centered Telemedicine and Decision Support System. In *HEALTHINF* (pp. 491-498).
16. Singh, S.P., Sharma, M.K., Lay-Ekuakille, A., Gangwar, D. and Gupta, S., 2020. Deep ConvLSTM with self-attention for human activity decoding using wearable sensors. *IEEE Sensors Journal*, *21*(6), pp.8575-8582.
17. Ghasemzadeh, H. and Jafari, R., 2013. Ultra-low-power signal processing in wearable monitoring systems: A tiered screening architecture with optimal bit resolution. *ACM Transactions on Embedded Computing Systems (TECS)*, *13*(1), pp.1-23.
18. Alinia, P., Saeedi, R., Fallahzadeh, R., Rokni, A. and Ghasemzadeh, H., 2016. A reliable and reconfigurable signal processing framework for estimation of the metabolic equivalent of the task in wearable sensors. *IEEE Journal of Selected Topics in Signal Processing*, *10*(5), pp.842-853.
19. Wang, L. and Liu, R., 2020. Human activity recognition is based on the wearable sensor using hierarchical deep LSTM networks. *Circuits, Systems, and Signal Processing*, *39*(2), pp.837-856.